RESEARCH ARTICLE | AUGUST 24 2022

Determination of base doping concentration of silicon solar cells from light *IV*-curves

Klaus Ramspeck ✉; Lothar Komp; Stefan Dauwe; ... et. al

AIP Conference Proceedings 2487, 030008 (2022)
https://doi.org/10.1063/5.0090130

Determination of Base Doping Concentration of Silicon Solar Cells from Light *IV*-curves

Klaus Ramspeck[1, a)], Lothar Komp[1], Stefan Dauwe[1], Karsten Bothe[2], David Hinken[2], Martin Wolf[2] and Michael Meixner[1]

[1]*h.a.l.m. elektronik GmbH, Friesstr. 20, 60388 Frankfurt a.M., Germany*
[2]*ISFH, Am Ohrberg 1, 31860 Emmerthal, Germany*

[a)] Corresponding author: k.ramspeck@halm.de

Abstract. In this contribution we present a novel method to determine the base doping concentration of solar cells from current-voltage (*IV)* curves measured under illumination. Our method is based on counting the charge carriers which are stored during an *IV*-sweep inside the Si bulk of the solar cell. We derive this charge from a comparison of a single sweep *IV*-curve and a steady-state *IV*-curve. Besides a detailed explanation of our new method, we analyze its applicability and repeatability and present an independent confirmation based on state-of-the-art capacitance-voltage (*CV*) characterization. We perform this confirmation of our results on a number of cells with different cell architectures ranging from p-type PERC solar cells over n-PERT cells to TOPCon and HJT structures. The base doping concentration determined by our method match the results of the reference *CV* measurements adequately with an approximate measurement uncertainty of 20%. In contrast to time consuming laboratory methods that require offline sample characterization, our evaluation is performed without the need of additional measurement equipment or measurement time and is ready for inline usage in solar cell mass production.

INTRODUCTION

As the doping concentration varies across Si crystal ingots, due to the segregation coefficient of dopants being smaller than 1, the doping concentration of silicon wafers used for solar cell production is not constant. The base doping concentration of silicon wafers is however a key parameter for the optimization of cell design and efficiency. It influences the passivation properties, contributes to the series resistance and affects the degradation behavior of the cells. Assessment of the base doping concentration in solar cell production allows to correlate the cell properties with incoming material properties and opens a path to more detailed solar cell modelling. Despite these numerous advantages, the base doping concentration is by now not routinely measured in solar cell production. While it can be easily measured on unprocessed wafers by four-point probe current voltage measurements [1], it is quite difficult to assess on finished solar cells. Methods used so far are mainly suited for laboratories [2] or require SunsVoc measurements [3]. Here we present a novel approach to determine the base doping concentration on solar cells using only routinely measured *IV*-curves. We describe the methodology of our new approach, present results on its applicability and repeatability on different cell architectures and carry out an independent confirmation of the base doping concentration determined. For the latter purpose, capacitance voltage measurements are performed at ISFH on a number of 22 samples using two different measurement setups available there. A short introduction into capacitance voltage measurements is included in this paper as far, as it is necessary for interpretation of the results presented here. This introduction to capacitance voltage measurements is given in the next section, before we explain our new method in detail.

SiliconPV 2021, the 11th International Conference on Crystalline Silicon Photovoltaics
AIP Conf. Proc. 2487, 030008-1–030008-8; https://doi.org/10.1063/5.0090130
Published by AIP Publishing. 978-0-7354-4362-4/$30.00

CAPACITANCE VOLTAGE MEASUREMENTS

A method, commonly used to determine the base doping concentration on finished solar cells is the capacitance voltage measurement [2]. In this measurement technique, the junction capacitance is determined by modulating a reverse voltage which is applied to the solar cell under test. The base doping concentration then relates to the junction capacitance via the equation

$$N_{\mathrm{dop}} = -\frac{2}{f^2 A_{\mathrm{macro}}^2 q \varepsilon_0 \varepsilon_{Si}} \left(\frac{\partial\, 1/C^2}{\partial V_{\mathrm{rev}}} \right)^{-1}, \tag{1}$$

where N_{dop} is the base doping concentration, C is the junction capacitance of the cell under test, V_{rev} the applied reverse voltage, q the elementary charge, ε_0 the vacuum permittivity and ε_{Si} the relative permittivity of Silicon. A_{macro} is the macroscopic cell area and f is an area enhancement factor which will be described in more detail below. Plotting the inverse squared junction capacitance as a function of the reverse voltage thus allows to determine the base doping concentration from the slope of this plot. For textured silicon a proportionality factor f^2 is required in eq. (1), which accounts for an area enhancement of the junction area compared to the cells' geometrical area [4,5]. This area enhancement is caused by the surface texture, which has a dimension, typically larger than the junction depth and thus increases the junction area. With increasing reverse voltage, the junction moves deeper into the silicon, the area enhancement factor therefore reduces for higher reverse voltages applied to the cell. An example of a capacitance voltage measurement of a textured solar cell is given in Fig. 1. An increase of the slope of the $1/C^2$ plot with increasing reverse voltage is observed, as the area enhancement factor reduces. While complicating the evaluation of the base doping concentration at first sight, this effect can be used to remove the area enhancement factor entirely from equation (1). Therefore, the value of the reverse voltage used in the measurement is increased until the slope of the curve saturates. In this condition, the junction of the solar cell has been moved deep enough into the silicon, to leave the region affected by surface texture. This behavior is modelled in ref. [6], such that the saturated value can be fitted from the slopes evaluated as a function of the reverse voltage. Therefore, using a setup with high enough reverse voltage, the area enhancement factor is removed from eq. 1 and the evaluation can be performed independent from the surface structure of the solar cell under test.

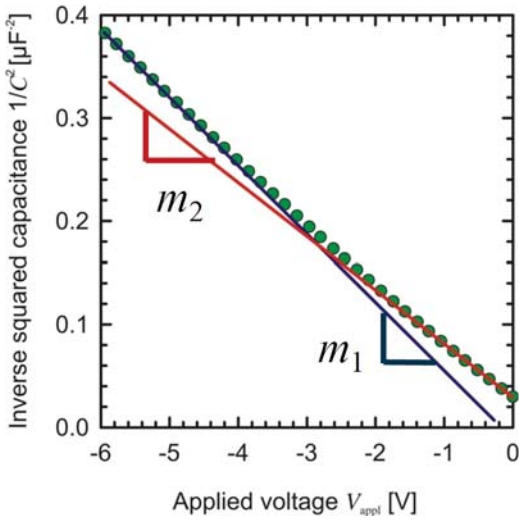

FIGURE 1. Inverse squared junction capacitance of a textured solar cell as a function of reverse voltage.

METHODOLOGY OF *IV*-CURVE BASED DETERMINATION OF WAFER DOPING

We base our method on a simple principle, what makes it applicable to all modern Si-solar cells. We count the minority charge carriers which are stored in the solar cells' volume during an *IV*-sweep and use the relation between junction voltage (V_j), minority carrier density (Δn) and base doping concentration (N_{dop}):

$$N_{dop} = -\frac{n_i^2}{\Delta n} exp\left(\frac{qV_j}{kT}\right) - \Delta n \tag{2}$$

In this equation derived easily from textbook knowledge [7], n_i is the intrinsic carrier concentration of silicon, k the Boltzmann constant and T is the temperature of the device. Using eq. (2), determination of the base doping concentration of a Si-solar cell reduces to the determination of the minority carrier density in the bulk of the solar cell at a known junction voltage. We propose a robust and easy approach based on the charge piling up inside the solar cell during an *IV*-curve measurement to determine this quantity. Due to limited measurement time in production, the *IV*-curve is measured at fast load sweep rates introducing transient effects in the measurement [8]. As a consequence, the measured *IV*-curves differ from the steady-state *IV*-curves. In production the steady-state *IV*-curve is commonly determined using the advanced hysteresis approach [8]. This approach provides three *IV*-curves, the measured curves in forward- and reverse-sweep direction and the steady-state curve calculated from them.

The difference between the current measured in a single-sweep *IV*-curve and the steady-state *IV*-curve is determined by the amount of charge carriers which are stored in the volume of the cell – reducing the current output in forward sweep direction and increasing it in reverse-sweep direction. Integrating the difference between the steady-state *IV*-curve and one of the sweeps thus yields the amount of charge carriers stored in the solar cell, the total charge Q. Figure 2(a) displays two *IV*-curves of a high-capacitance hetero junction solar cell. The $I_{SC} \rightarrow V_{OC}$ curve, measured with a sweep time of 30 ms, is shown in blue and the steady-state *IV*-curve is displayed in red. The yellow marked difference between these two curves is additionally displayed in Fig. 2(b). It is the charging current of the solar cell which accumulates minority charge carriers in the bulk of the cell. The charging current reaches a maximum value of approximately 650 mA for the case demonstrated here at a voltage of about 635 mV. At higher voltages, the charging current decreases again, due to a reduced sweep speed of the $I_{SC} \rightarrow V_{OC}$ sweep at higher voltages. Integrating the charging current in the time domain of the forward sweep, the total charge of the solar cell under test is obtained in the unit of coulombs. Figure 3(a) displays this charge during the measurement time of the sweep from Figure 2. At 735 mV, the cells V_{OC}, a total charge of more than 6 mC is achieved.

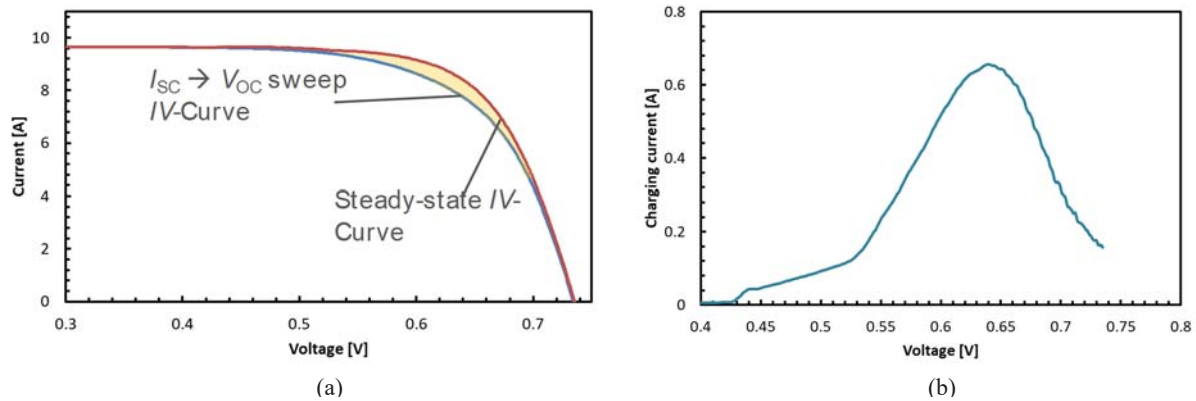

FIGURE 2. (a) Single sweep *IV*-curve and steady-state *IV*-curve of a hetero junction silicon solar cell. The single sweep is performed in 30 ms sweep time. (b) The difference between the two *IV*-curves is the charging current which accumulates minority carriers in the silicon cell during the *IV*-sweep.

In order to derive the base doping concentration from the charge stored in the solar cell during an *IV*-sweep, two further steps are necessary. First of all, the total charge needs to be converted into the excess minority carrier density. Therefore, we use the geometrical parameters of the cell, it's thickness (w) and its surface area (A)

$$\Delta n = \frac{Q}{A\, w\, q} \tag{3}$$

The resulting minority carrier density is still given as a function of the measured cell voltage. However, in eq. (2), the junction voltage is required to derive the base doping concentration. For this reason, the measured voltage (V) is translated into the junction voltage (V_j), correcting for the voltage drop at the series resistance (R_{ser})

$$V_j = V + R_{ser}\, I \tag{4}$$

The resulting minority carrier density as a function of the cells junction voltage is displayed in Fig. 3(b) for the exemplary HJT-cell measurement evaluated here. The determined minority carrier concentration spans the range from 10^{12} cm^{-3} at 400 mV junction voltage up to 2x10^{16} cm^{-3} at V_{OC} of this cell at around 735 mV. A bump is visible around 480 mV junction voltage, which is caused by a slight deviation of the steady-state IV-curve from its expected form at this voltage. Above approximately 520 mV, the minority carrier density follows an exponential increase.

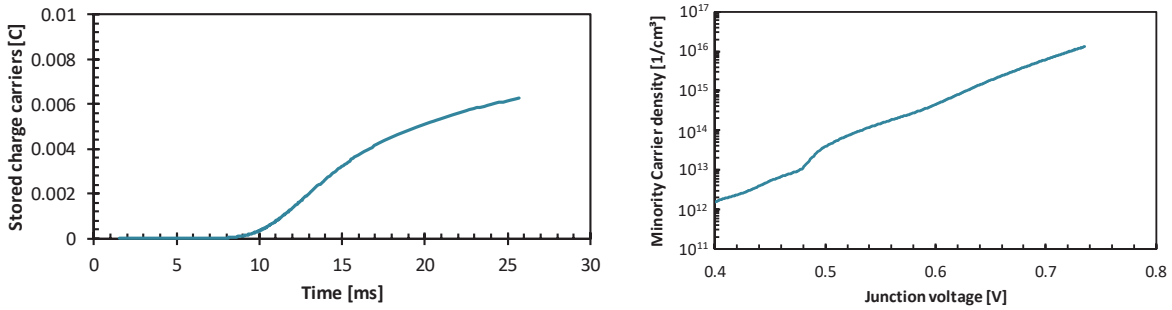

(a) (b)

FIGURE 3. (a) Accumulation of stored charge carriers as a function of sweep time. (b) Minority carrier density as a function of the cells' junction voltage.

Using eq. (2), the base doping concentration is calculated from the minority carrier density for each junction voltage. In this way, a complete base doping concentration curve is obtained. This curve is plotted, transformed back to the measured voltage V, in Fig. 4. Above a voltage of 550 mV, the resulting base doping concentration is observed to be a constant value, as would be the expected behavior. At smaller voltages it becomes instable, indicating, that the low charge carrier concentration in this range cannot be evaluated safely. The final determination of the base doping concentration value for the cell is done taking the average over an evaluation range in which the result is approximately constant and yields 2.08x10^{15} cm^{-3} for this cell. Throughout the calculation outlined in this paper, some parameters are required to be fitted, which is done self-consistently, using the mean square error sum of the deviation of the actual base doping concentration curve from its mean value in the evaluation range. The parameters which are fitted are of

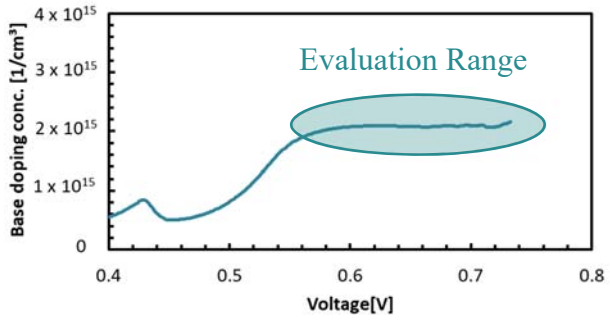

FIGURE 4. Base doping concentration of a HJT solar cell as a function of the cell voltage. Below approximately 550 mV the signal for the evaluation is too small and the base doping values evaluated are not valid.

technical nature and the fitting is done self-consistently, no parameters need to be determined ahead besides the geometrical cell information. This self-consistency is achieved with just one simple assumption; the base doping concentration should not be a function of the cell voltage. It is possible, only because a complete base doping concentration curve is evaluated and not just one value at a single point on the curve.

VALIDATION AND MEASUREMENT RESULTS

To validate our newly developed method, we use three steps. First we perform the evaluation on cells with different cell architectures to verify its applicability on a broad range of samples. Then we evaluate the repeatability on cells with different cell architectures including a variation of the sweep time for the single-sweep *IV*-curve which is used in the data analysis. Finally, we perform an independent validation of the measurement results using capacitance voltage measurements [4-6] performed at ISFH as a reference.

In the first step, we evaluate *IV*-curves from a mc-Si BSF cell with low capacitance, where we expect a low evaluation signal, from a p-type PERC cell, a n-PERT cell and a HJT cell. Figure 5 displays the resulting base doping concentration curves for these four cells, again as a function of the measured voltage *V*. For all cells, a sufficient evaluation range with constant base doping concentration is observed, which demonstrates the wide range of applicability of our method. For voltages above approximately 500 mV, the evaluation can be performed, with only the HJT cell requiring slightly higher voltages. In our four examples, we evaluate base doping concentrations of 1.55×10^{16} cm^{-3} for the mc-BSF cell, 6.16×10^{15} cm^{-3} for the PERC cell, 3.15×10^{15} cm^{-3} for the n-PERT and 2.19×10^{15} cm^{-3} for the HJT cell.

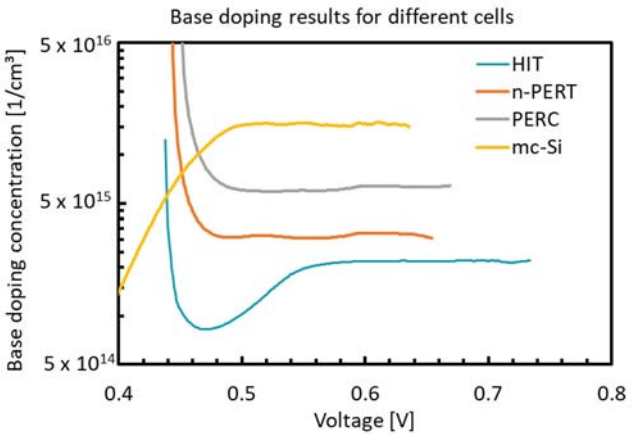

FIGURE 5. Base doping concentration as a function of cell voltage for 4 cells with different cell architectures.

Having proven the applicability of our method for the different cell architectures, an analysis of the repeatability of the measurement results is carried out next. Here, simple repeatability measurements are performed using a HJT, a PERC, a n-PERC and a TOPCon cell. In addition, a combined repeatability with sweep-time variation is performed using PERC cells of different manufacturers, n-PERT cells and a mc-Si BSF cell as small signal test object. For these cells, measurements are performed using 4.3 ms, 8.5 ms and 16 ms sweep time for the single sweep measurement.

All results of this repeatability examination are given in Fig. 6. The colored bars in the image mark the individual cells, the colors of the bars mark the different cell architectures. Open circles mark the results from the pure repetition experiment, while filled symbols represent the sweep time variation and repetition. In the latter, light blue triangles are the results of 4.3 ms sweep time, darker blue quadrats of 8.5 ms sweep time and dark blue circles show the results from 16 ms sweep time. For all cells examined, the difference between the maximum and minimum result for the base doping concentration is smaller than 10% relative, except for the mc-Si BSF solar cell. In this case, two results deviate from the others, which are the measurements performed with a sweep-time of 16 ms. For such low capacitance cells and high sweep-time, the remaining transient effect in the single sweep measurement is too small for a precise determination of the base doping concentration, causing the higher deviation for this cell. This demonstrates the applicability limit of our new method, which might be concentrated to the statement that cells with open circuit voltage

above approximately 630 mV are required in order to effectively use the transient effects for this kind of base doping concentration determination.

For the other cells, repeatability is not affected significantly by the variation of the sweep time in the given limits. It should however be noted, that the very short sweep times in the examination could not be used for very high capacitance cells, which require sweep times above approximately 15 ms.

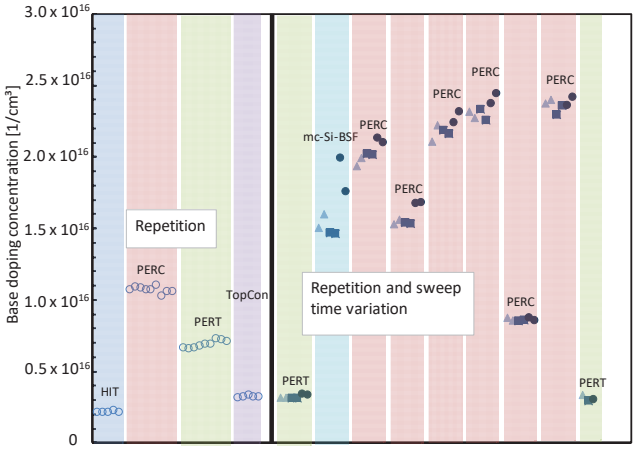

FIGURE 6. Results of measurement repeatability and sweep time variation for a number of Si-solar cells with different cell architectures. Individual cells are marked by the colored bars, the colors mark the cell architectures. Open symbols represent pure repetition measurements, filled symbols the sweep time variation and repetition. In the latter, bright blue triangles show 4.3 ms sweep time results, darker blue quadrats 8.5 ms sweep time results and dark blue circles the 16 ms sweep time results.

With the applicability on different cell architectures, as well as the repeatability of the measurement results being tested, the final and most important test of our new method is the comparison with reference measurements in order to investigate whether the results we obtain in a repeatable way are the correct values of the base doping concentration or not.

For this reason, we perform IV-measurements on 22 cells and determine their base doping concentration from the resulting IV-curves. Table 1 gives an overview over the samples used for the reference measurements. These cells were sent to ISFH where they were measured using two capacitance voltage measurement setups, working in different voltage ranges. One setup which we name “low voltage setup” works in a voltage range down to -5 V and requires an area correction factor for the evaluation, as outlined in the section on capacitance voltage measurements. The second setup uses reverse voltages down to -25 V and therefore does not require an area enhancement factor. On this high-voltage setup, not all the samples could be measured, due to technical issues and low junction breakdown voltages for some of the samples.

TABLE 1. Overview over sample solar cells used for independent confirmation of the new base doping measurement method.

Cell type	Number of cells	Number of manufacturers
HJT	3	1
TopCon	3	1
p-Type PERC	9	3
n-PERT	7	2

In order to obtain a reliable reference measurement value for all samples, the area enhancement factor for the low voltage setup is set to optimize the agreement between the measurement results on both capacitance voltage setups, yielding an average value of $f = 1.1$. This value fits alkaline textures with a pyramid height of about 3 µm and an emitter depth between 200 nm and 400 nm. The agreement between the results from both setups using this factor for all cells is displayed in Fig. 7(a), where the doping concentrations obtained from the measurements on the low voltage setup are displayed on the x-axis and the doping concentrations achieved from the measurements on the high voltage setup are displayed on the y-axis. A red line is drawn to mark the perfect one-to-one correlation in the graph. All measurement values agree well within the error boundaries of +/-20% relative. With this result, the measurements on the low voltage setup are validated for the area enhancement factor of 1.1, allowing to use the results of this setup in the confirmation of our new method for all cells, which could not be measured on the high voltage setup. The final result of the independent confirmation is then displayed in Fig. 7(b). Here, the doping concentrations derived from the capacitance voltage measurements are displayed on the x-axis, while the results we achieve from the analysis of the *IV*-curves are given on the y-axis. Again, a red line is drawn to mark the perfect one to one correlation. The agreement between the results from both methods is found to be remarkably good, with nearly all values agreeing within the given uncertainty ranges. This is true for the whole, large range of doping concentrations spanned by the samples in the confirmation measurements, ranging from 10^{15} cm^{-3} up to $3\text{x}10^{16}$ cm^{-3}. The agreement of the results of the two different methods is nearly as good as the agreement between the two capacitance voltage measurement setups and only a few cells with lower doping concentration show a difference which is as large, as the relative error associated with the measurement. This result clearly demonstrates, that our new method to determine the base doping concentration of solar cells from light *IV*-curves measured routinely in solar cell production is applicable for a broad range of cell architectures, base doping concentrations and delivers correct and repeatable results.

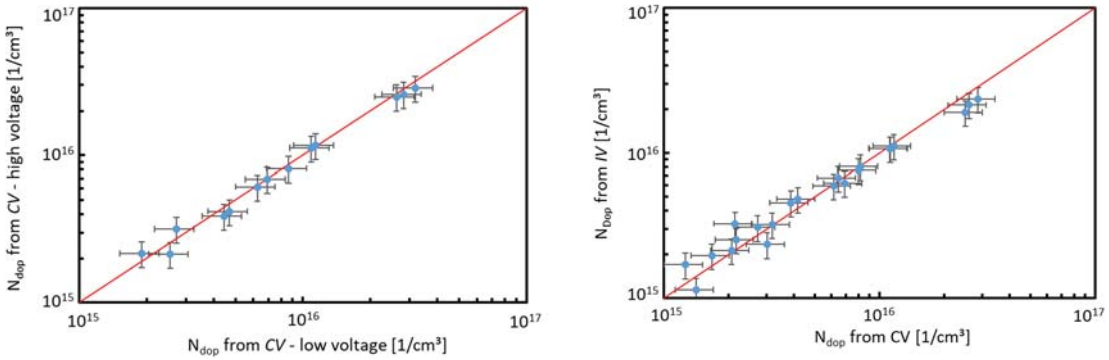

FIGURE 7. (a) Agreement between the measurement results of the two capacitance voltage measurement setups at ISFH, assuming an area enhancement factor of 1.1 for all measurements on the low voltage setup. (b) Results of the independent confirmation of base doping concentrations derived from *IV*-measurements using capacitance voltage measurements.

CONCLUSIONS

We presented a novel method for the determination of the base doping concentration on finished solar cells, using only light *IV*-curves routinely measured in high-volume solar cell production. The method is based on the hysteresis effect caused by the accumulation of minority carriers in the volume of a solar cell during an *IV*-sweep, which is evaluated quantitatively using the steady-state *IV*-curve derived from advanced hysteresis analysis. From the difference between the steady-state and the single sweep *IV*-curves, the minority carrier density is derived, which is then used to determine the base doping concentration using the junction voltage as additional input. Delivering not only one single value for the base doping concentration, but a base doping concentration curve as a function of the cells voltage, a self-consistent evaluation is performed in the higher voltage range, where the difference between the *IV*-curves is large enough for the evaluation, aiming at a constant base doping value for all voltages in the evaluation range, as commonly the base doping concentration is not expected to be a function of the applied voltage.

We test our method on a number of different cell architectures and perform an analysis of the measurement repeatability as well, as an independent confirmation using capacitance voltage measurements performed at ISFH as a reference. For this confirmation, 22 samples are used, covering a wide range of base doping concentrations from 10^{15} cm^{-3} to $3x10^{16}$ cm^{-3} with four different cell architectures and cells from many different suppliers. As shown, a very good agreement among the different methods is achieved, proving the applicability of our new method, which allows for total production base doping monitoring in high-throughput solar cell production without the requirement for additional measurement equipment or measurement time.

REFERENCES

1. S.M. Sze, *Semiconductor devices: Physics and Technology* (John Wiley & Sons, 2nd edition, 2002), p. 54.
2. D. K. Schroder, *Semiconductor material and device characterization* (Wiley-IEEE Press, 2015), pp. 61ff.
3. A. L. Blum, R. A. Sinton, W. Dobson, H. Wilterdink and J. H. Dinger, "Lifetime and substrate doping measurements of solar cells and application to in-line process control" in Proc. of IEEE 43rd Photovoltaic Specialists Conference (PVSC) (Portland, OR, 2016) pp. 3534-3537.
4. F. Recart and A. Cuevas, IEEE Transactions on Electron Devices, **53,** 442-448 (2006).
5. D. Hinken, A. Milsted, R. Bock, B. Fischer, K. Bothe, M. Schütze, J. Isenberg, A. Schulze and M. Wagner, IEEE Transaction on Electron Devices, **57,** 2831-2837 (2010).
6. M. Schuetze, D. Hinken, A. Milsted, M.B. Koentopp and K. Bothe, IEEE Transactions on Electron Devices **58**(11), 3759 - 3770, (2011).
7. M.A. Green, *Solar Cells – Operating principles, Technology and System Applications*, (Prentice-Hall Inc., 1982), p. 70.
8. K. Ramspeck, S. Schenk, L. Komp, A. Metz and M. Meixner, "Accurate efficiency measurements on very high efficiency silicon solar cells using pulsed light sources", Proc. of the 29th EU-PVSEC, (Amsterdam, 2014), pp. 1253 – 1256.